



Selective oxidation of CH₄ to CH₃OH through plasma catalysis: Insights from catalyst characterization and chemical kinetics modelling

Yanhui Yi^{a,b,*}, Shangkun Li^{a,b,1}, Zhaolun Cui^b, Yingzi Hao^a, Yang Zhang^c, Li Wang^d, Pei Liu^e, Xin Tu^f, Xianming Xu^g, Hongchen Guo^a, Annemie Bogaerts^b

^a State Key Laboratory of Fine Chemicals, School of Chemical Engineering, Dalian University of Technology, Dalian, 116024, PR China

^b Research Group PLASMANT, Department of Chemistry, University of Antwerp, Universiteitsplein 1, BE-2610, Wilrijk, Antwerp, Belgium

^c School of Materials Science and Engineering, Center of Advanced Analysis & Gene Sequencing, Zhengzhou University, Zhengzhou, 450001, PR China

^d College of Environmental Sciences and Engineering, Dalian Maritime University, Dalian, 116026, Liaoning, PR China

^e In-situ Center for Physical Sciences, School of Chemistry and Chemical Engineering, Shanghai Jiao Tong University, Shanghai, 200240, PR China

^f Department of Electrical Engineering and Electronics, University of Liverpool, Liverpool, L693GJ, UK

^g Daqing Chemical Research Center, China National Petroleum Corporation, Daqing, 163714, PR China

ARTICLE INFO

Keywords:

Methane conversion
Plasma catalysis
Selective oxidation
Methanol synthesis
Plasma chemistry

ABSTRACT

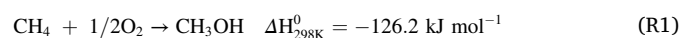
The selective oxidation of methane to methanol (SOMTM) by molecular oxygen is a holy grail in catalytic chemistry and remains a challenge in chemical industry. We perform SOMTM in a CH₄/O₂ plasma, at low temperature and atmospheric pressure, promoted by Ni-based catalysts, reaching 81 % liquid oxygenates selectivity and 50 % CH₃OH selectivity, with an excellent catalytic stability. Chemical kinetics modelling shows that CH₃OH in the plasma is mainly produced through radical reactions, i.e., CH₄ + O(1D) → CH₃O + H, followed by CH₃O + H + M → CH₃OH + M and CH₃O + HCO → CH₃OH + CO. The catalyst characterization shows that the improved production of CH₃OH is attributed to abundant chemisorbed oxygen species, originating from highly dispersed NiO phase with strong oxide support interaction with γ-Al₂O₃, which are capable of promoting CH₃OH formation through E-R reactions and activating H₂O molecules to facilitate CH₃OH desorption.

1. Introduction

Methane (CH₄), abundant in natural gas, shale gas, coalbed gas, biogas and dry gas (i.e., emission of chemical industry), has become not only an important source of clean fossil energy, but also a feedstock for the chemical industry. At present, the industrial utilization of CH₄ is initiated by high temperature steam reforming to syngas (CO and H₂), which is then transformed into hydrocarbons through the Fischer-Tropsch process, or into methanol (CH₃OH), through a high-pressure reaction over Cu-Zn-Al catalyst. CH₃OH is a versatile molecule for the production of many bulk chemicals, such as ethylene, propylene and aromatics [1]. However, due to the strong C–H bond energy (439 kJ/mol), the negligible electron affinity and low polarizability of CH₄, as well as thermodynamic limitations, the syngas pathway is energy intensive and costly, which stimulates researchers to develop novel approaches for the conversion of CH₄. Thus, the selective oxidation of methane to methanol (SOMTM) is attracting more and more attention

[2,3].

SOMTM is being studied by homogeneous catalysis, in strong acid media (sulfuric and trifluoroacetic acid), using complex catalysts with noble metals (Pt and Pd) as central atoms [4–6]. Alternatively, SOMTM can also be realized by impressive heterogeneous catalysis, e.g. iron-based zeolites [7,8] and copper-based zeolites [9–11], or supported noble metals, such as Au, Pd and Rh [12,13]. However, numerous works in homogeneous or heterogeneous catalysis adopted high price oxidants such as N₂O or H₂O₂, which made this process economically infeasible in large-scale application. Using the abundant and cheap molecular oxygen (O₂) as oxidant, (R1), would be highly desirable in industrial application.



SOMTM by O₂, R1, has been extensively studied. Colloidal Au-Pd nanoparticles exhibited high CH₃OH selectivity (92 %) in aqueous solution at mild temperatures on SOMTM with H₂O₂ and O₂ as oxidants.

* Corresponding author.

E-mail address: yianhui@dlut.edu.cn (Y. Yi).

¹ These authors contributed equally (shared first authors).

<https://doi.org/10.1016/j.apcatb.2021.120384>

Received 2 March 2021; Received in revised form 13 May 2021; Accepted 18 May 2021

Available online 21 May 2021

0926-3373/© 2021 Elsevier B.V. All rights reserved.

More oxygenated products were formed than the amount of H_2O_2 consumed, suggesting that the controlled breakdown of H_2O_2 activates methane, which subsequently incorporates molecular oxygen through a radical process [12]. $\text{CeO}_2/\text{Cu}_2\text{O}$ catalysts were able to activate methane at room temperature, and water addition could generate centers on the catalyst surface with special electronic properties, on which methane can directly interact to yield methanol [14,15]. Recently, highly active Au-Pd nanoparticles were encapsulated inside zeolites and modified with a hydrophobic sheath, which can considerably enhance the oxidation of methane to methanol [16]. The silanes appeared to allow diffusion of H_2 , O_2 , and CH_4 to the catalyst active sites, while confining the in-situ generated H_2O_2 decomposition, which provided a high local peroxide concentration to facilitate methanol production, with 17.3 % methane conversion and 92 % methanol selectivity. Additionally, chemical looping was also proposed to inhibit methane overoxidation on Cu- or Fe- containing zeolite catalysts [17].

Although great progress has been reported, SOMTM is, currently, still being considered as a dream reaction in chemical industry and a holy grail in catalytic chemistry [3,17,18]. Generally, it has to overcome two challenges, caused by thermodynamics and kinetics, respectively. The first is how to improve the CH_3OH selectivity. Thermodynamically, CH_3OH is not the favorable product, as CO and CO_2 are more stable than CH_3OH . Specifically, as shown in Fig. S1, a low temperature (< 890 K) favors the production of CO_2 and H_2O , while a high temperature (> 890 K) favors CO and H_2 . In other words, due to the higher reactivity of CH_3OH than the feedstock CH_4 , the catalytic sites, capable of oxidizing CH_4 into CH_3OH , can also further oxidize CH_3OH into CO or CO_2 before CH_3OH can desorb from the catalyst surface. The second challenge is how to reduce the kinetic energy barrier (E_a) of SOMTM by O_2 at ambient conditions. The E_a of SOMTM by O_2 is much higher than for SOMTM using N_2O or H_2O_2 as oxidants, because both N_2O and H_2O_2 can more easily release an oxygen atom, as the main species to trigger the oxidation of CH_4 to CH_3OH . Therefore, when using O_2 as oxidant, high temperature and high activity catalysts are needed to overcome the E_a of SOMTM, which unfortunately leads to deep oxidation.

One approach to overcome the above-mentioned challenges is a stepwise process, i.e., stoichiometric chemical looping, which involves three separate steps: (1) activation of the metal-zeolite catalyst by an oxidant at a relative high temperature (250–500 °C), (2) methane reaction at a relative low temperature (25–200 °C), and (3) methanol extraction using a solvent or steam at a relative low temperature (25–200 °C) [9,19,20]. Currently, Cu and Fe exchanged zeolites have been extensively studied, and significant attention was given to the elucidation of the nature of copper-oxo and iron-oxo active sites [17, 20]. However, the state-of-the-art conversion of methane to methanol via chemical looping stays a factor ~ 50 below the industrial threshold in an overall production rate, and improvement on material productivity and decreased cycle time are highly needed for this process [21].

Another approach to overcome the above-mentioned challenges is plasma catalysis. Non-thermal plasma (NTP), which is an ionized gas with clear non-equilibrium character, offers a distinct approach to activate molecules by energetic electrons instead of heat, and thus triggers chemical reactions at low temperature [22–27]. Generally, the gas temperature in NTP remains near room temperature, while the generated electrons exhibit a typical temperature of 1–10 eV ($\sim 10^4$ – 10^5 K), which is sufficient to activate feed gas molecules (e.g., CH_4 and O_2) into reactive species, including radicals, excited atoms and molecules, and ions. Several scientists have studied SOMTM by O_2 through plasma and/or plasma catalysis [28–36], but only a few have reported satisfying CH_3OH selectivity. Nozaki applied a microplasma and obtained a CH_4 conversion to synthetic fuels with maximum organic liquid selectivity of 70 % without catalysts (plasma alone) [28], but the CH_3OH selectivity was below 15 %. Indarto realized CH_3OH synthesis with optimum selectivity of 23 % using a dielectric barrier discharge (DBD) reactor with Ni metal doped over yttria-stabilized zirconia as catalyst [29]. Chawdhury used a packed bed DBD reactor, in which glass beads

provided an optimal CH_3OH selectivity of 35.4 % [30], while further work reported the best CH_3OH selectivity of 37 % using $\text{CuO}/\gamma\text{-Al}_2\text{O}_3$ catalyst [31]. Recently, $\text{Cu}/\gamma\text{-Al}_2\text{O}_3$, $\text{Ni}/\gamma\text{-Al}_2\text{O}_3$ and $\text{Fe}/\gamma\text{-Al}_2\text{O}_3$ catalysts were compared for plasma-catalytic methane to value-added liquid fuels and chemicals, in which the highest liquid oxygenate (~ 71 %) were achieved, with $\text{Fe}/\gamma\text{-Al}_2\text{O}_3$ catalyst exhibited highest methanol selectivity of 36.0 % among three different catalysts [32]. In addition, the insights from microkinetic modelling for plasma-catalytic SOMTM process were obtained on Pt(111) surface and the results showed that vibrational excitation and especially radicals produced from CH_4/O_2 NTP could enhance the turnover frequency (TOF) and improve the selectivity of CH_3OH , HCOOH and C_2 hydrocarbons [33]. In general, this field is still in the early research stages and fundamental information on the interaction of NTP with a catalyst is still lacking, and the limited CH_3OH selectivity in most studies is attributed to the further oxidation of CH_3OH into CO and CO_2 [34]. Additionally, the reaction pathway for the production of CH_3OH and by-products (HCHO , HCOOH , CO and CO_2) from CH_4 and O_2 in NTP is largely unknown.

Inspired by Lustemberg's work that Ni- CeO_2 catalysts shows excellent activity in SOMTM at moderate conditions [37], in this paper, we report SOMTM in a CH_4/O_2 plasma promoted by Ni-based catalysts, with 50 % selectivity to CH_3OH , and total liquid oxygenates selectivity of 81 %, and with excellent catalytic stability. In addition, we identify the underlying reaction mechanisms by combined experiments and modeling.

2. Experimental section

2.1. Catalyst preparation

The catalysts were synthesized by the incipient wetness impregnation method (Scheme S1). Commercial $\gamma\text{-Al}_2\text{O}_3$ pellets (1–2 mm diameter), synthesized by a hydrothermal method, were calcined at 400 °C in a muffle oven for 5 h before they were used as supports. All analytical grade chemicals were purchased from Tianjin Kemiou Chemical Reagent Co. Ltd. (Tianjin, China) and used without further purification. The preparation procedure of the Ni catalysts is described in Scheme S2: First, the precursor salt $\text{Ni}(\text{NO}_3)_2 \cdot 6\text{H}_2\text{O}$ was dissolved in deionized water, followed by the addition of $\gamma\text{-Al}_2\text{O}_3$ pellets under stirring. After 12 h aging at room temperature, the sample was dried at 120 °C overnight. Finally, the sample was calcined by a muffle oven at 540 °C for 5 h in air condition, and the catalyst was noted as $\text{NiO}/\gamma\text{-Al}_2\text{O}_3$. Varied nickel loading, i.e., 2, 6, 10, 15, 20, and 25 wt.% catalysts were synthesized based above method.

2.2. Experimental setup

The experimental plasma catalysis setup is shown in Scheme S2. The plasma catalytic SOMTM by O_2 was carried out using a coaxial DBD reactor with a novel water electrode (grounding electrode) at atmospheric pressure. The DBD reactor consists of a pair of coaxial quartz cylinders (inner and outer quartz tubes) in which a stainless-steel (2 mm outer diameter) electrode was placed in the center, and circulating water was pumped into the space between the inner and outer cylinder. A tungsten filament is installed in between both cylinders to connect this circulating water (flowing between this inner and outer wall) with a ground wire (outside of the reactor wall), so that the circulating water acts as a ground electrode of our DBD. The flow rate (6 L/min) and temperature of water was controlled by thermostatic baths with a circulation pump and external temperature controller, which can effectively remove the heat generated by the discharge and maintain a constant reaction temperature. The discharge length is 50 mm (defined by the length of the ground electrode, i.e., region of circulating water) and the inner diameter of the inner quartz cylinder is 10 mm, yielding a discharge gap of 4 mm. In the plasma catalysis experiments, the discharge space was fully packed by 1.25 g catalyst. CH_4 and O_2 were

monitored by calibrated mass flow controllers and mixed homogeneously before passing through the plasma reactor. Before igniting the discharge, this gas mixture passed through the plasma reactor for about 10 min to remove air, to ensure a safe operating procedure (outside the explosion limit). The change of gas volume after the reaction was measured using a soap-film flow meter. This is needed to quantitatively analyze the gas composition, and to achieve the exact conversion (CH_4) and selectivity of the gaseous products (CO and CO_2). The discharge voltage and current were detected by a digital phosphor oscilloscope (Tektronix, DPO 3012) with a high voltage probe (Tektronix P6015) and a current probe (Pearson 6585).

The feedstock and gas products were analyzed by an on-line gas chromatograph (Tianmei GC-7900, TDX-01 column, Al_2O_3 packed column) with a thermal conductivity detector (TCD) and a flammable ionized detector (FID). The liquid products were cooled by a liquid trap (mixer of isopropyl alcohol and liquid nitrogen, below -120°C) and then analyzed by GC-2014C (Shimadzu, PEG-2000 column), GC-MS (Agilent 5975C, DB-1701 column), FTIR (ThermoFisher 6700) and $^1\text{H-NMR}$ (Bruker AVANCE III 500). The reaction products, including H_2O , CO , CO_2 , CH_3OH , HCHO , HCOOH , HCOOCH_3 , $\text{C}_2\text{H}_5\text{OH}$, CH_3CHO , and CH_3COOH , were analyzed using external standards. The gas products were measured by gas chromatography, while the liquid products were collected by a liquid trap and analyzed by GC, GC-MS, FTIR and $^1\text{H-NMR}$ (Fig. S2). The formulas of the standard calibrated concentration curves are shown in Table S1. More details about qualitative and quantitative analysis of products on CH_4/O_2 NTP could be found in supporting information. In this work, the conversion of CH_4 and the selectivity of the gaseous products (CO_x , H_2 and C_2H_6) are calculated as follows. Note that the selectivity of CO_x and C_2H_6 is calculated based on carbon, while the selectivity of H_2 and H_2O is calculated based on hydrogen.

The CH_4 conversion was calculated by:

$$X_{\text{CH}_4} (\%) = \frac{\text{moles of CH}_4 \text{ converted}}{\text{moles of initial CH}_4} \times 100 \% \quad (1)$$

The selectivity of the gaseous products was calculated as :

$$S_{\text{CO}} (\%) = \frac{\text{moles of CO produced}}{\text{moles of CH}_4 \text{ converted}} \times 100 \% \quad (2)$$

$$S_{\text{CO}_2} (\%) = \frac{\text{moles of CO}_2 \text{ produced}}{\text{moles of CH}_4 \text{ converted}} \times 100 \% \quad (3)$$

$$S_{\text{H}_2} (\%) = \frac{\text{moles of H}_2 \text{ produced}}{2 \times \text{moles of CH}_4 \text{ converted}} \times 100 \% \quad (4)$$

$$S_{\text{H}_2\text{O}} (\%) = 100 \% - (S_{\text{CH}_3\text{OH}} + S_{\text{HCHO}} + S_{\text{HCOOH}} + S_{\text{H}_2} + S_{\text{C}_2}) \quad (5)$$

$$S_{\text{C}_2\text{H}_6} (\%) = \frac{2 \times \text{moles of C}_2\text{H}_6 \text{ produced}}{\text{moles of CH}_4 \text{ converted}} \times 100 \% \quad (6)$$

The selectivity of the liquid products was calculated as follows:

$$\text{Total selectivity of liquid products } (\%) = 100 \% - (S_{\text{CO}} + S_{\text{CO}_2} + S_{\text{C}_2\text{H}_6}) \quad (7)$$

The selectivity of the various oxygenates, $\text{C}_x\text{H}_y\text{O}_z$, can be calculated as:

$$S_{\text{C}_x\text{H}_y\text{O}_z} (\%) = \frac{X \times N_{\text{C}_x\text{H}_y\text{O}_z}}{\sum X_i N_i} \times \text{eq5} \quad (8)$$

Where $N_{\text{C}_x\text{H}_y\text{O}_z}$ represents the number of moles of various oxygenates in the liquid fraction. Note that we define here the carbon-based selectivity, and thus, H_2O and H_2O_2 are not included in this formula.

The corresponding yields of these $\text{C}_x\text{H}_y\text{O}_z$ oxygenates are calculated as:

$$Y_{\text{C}_x\text{H}_y\text{O}_z} (\%) = S_{\text{C}_x\text{H}_y\text{O}_z} (\%) \times X_{\text{CH}_4} (\%) \quad (9)$$

Finally, we defined the energy efficiency for CH_3OH formation (mol/kwh) as :

$$\text{Energy efficiency} = \frac{\text{moles of methanol produced (mol/h)}}{\text{discharge power (kW)}} \quad (10)$$

2.3. Catalyst characterization and NTP diagnostics

The structural properties of the $\text{NiO}/\gamma\text{-Al}_2\text{O}_3$ catalysts were investigated by X-ray diffraction (XRD), conducted using a SmartLab 9 kW diffractometer with $\text{Cu K}\alpha$ radiation (240 kV, 50 mA). The H_2 -temperature programmed reduction (H_2 -TPR) was performed on a Quanta chrome ChemBET Pulsar Chemisorption instrument. Before the analysis, the samples (0.20 g) were pretreated with He from ambient temperature to 150°C , and kept at 150°C for 60 min. Afterward, the samples were cooled to 50°C in He atmosphere. Finally, the H_2 -TPR was carried out in a flow of H_2/Ar mixture (120 mL/min, 10% H_2) from 100°C to 1000°C at a heating rate of $10^\circ\text{C}/\text{min}$. X-ray photoelectron spectroscopy (XPS) was conducted by Thermo Fisher ESCALAB XI⁺ with $\text{Al K}\alpha$ X-ray source. The C 1s binding energy value (284.8 eV) was taken as a reference level. Nitrogen physisorption was conducted on a Micromeritics ASAP 2020 instrument at -196°C to obtain textural information. Prior to the measurement, the samples were degassed at 400°C for 6 h. The surface area was calculated by the BET method and the pore volume was obtained by the t-plot method. The chemical composition of the $\text{NiO}/\gamma\text{-Al}_2\text{O}_3$ catalysts with various loading was analyzed by X-ray fluorescence (XRF) on S8 TIGER from Bruker AXS. Thermogravimetry was conducted by Netzsch STA 449 F3 connected to a Balzers QMG 403D mass spectrometer. High-resolution transmission electron microscopy (HRTEM) was conducted on Tecnai G2 F30 S-Twin with 300 kV accelerating voltage. High angle annular dark field scanning transmission electron microscopy (HAADF-STEM) was performed by Titan³™ G2 60–300 with Cs-corrector configuration. The CH_4/O_2 NTP was investigated by optical emission spectroscopy (OES) through a spectrograph (SP2758, Princeton instrument company). A fiber was directly connected at the wall of the plasma reactor, to detect the emission, which was analyzed by a spectrograph (750 mm, 300 G/mm gratings). A CCD (PIXIS:400-BR_eXcelon) was used to record the spectra with an on-line computer.

3. Results and discussion

3.1. Catalytic performance

As shown in Fig. 1A, the CH_4 conversion is zero when using only the $\text{NiO}/\gamma\text{-Al}_2\text{O}_3$ catalyst in the absence of NTP, indicating that SOMTM by O_2 cannot be triggered over $\text{NiO}/\gamma\text{-Al}_2\text{O}_3$ catalyst without help of NTP. In plasma alone, 4.1 % CH_4 conversion is achieved with 42.2 % CH_3OH selectivity, and no hydrocarbons have been detected by the GC. Hence, plasma alone is able to quite selectively produce CH_3OH in our setup, while it is generally stated in literature that it is not selective at all, and needs a catalyst for the selective production of target compounds [22, 34]. This is attributed to the short residence time, as will be explained by the modeling results below. Furthermore, the influence of NTP (CH_4/O_2 molar ratio, temperature of grounding electrode, discharge power and residence time) was also been studied, as shown in Figs. S3–S6. After packing by $\gamma\text{-Al}_2\text{O}_3$, the CH_4 conversion is slightly enhanced to 4.6 %, while the CH_3OH selectivity is reduced to 41.4 %. However, when using $\text{NiO}/\gamma\text{-Al}_2\text{O}_3$ catalyst (10 wt.% loading), the CH_4 conversion and CH_3OH selectivity increase to 6.4 % and 49.7 %, respectively, indicating that $\text{NiO}/\gamma\text{-Al}_2\text{O}_3$ catalyst has a positive effect on the CH_3OH production in CH_4/O_2 NTP. The CH_4 conversion is still limited, attributed to the short residence time of the gas inside the DBD reactor (high space velocity). By tuning the flow rates and other discharge conditions, it should be possible to enhance the conversion, but in this paper, we mainly focus on inhibiting the CH_4 overoxidation, to increase the liquid oxygenates selectivity, especially for CH_3OH production. The complete product

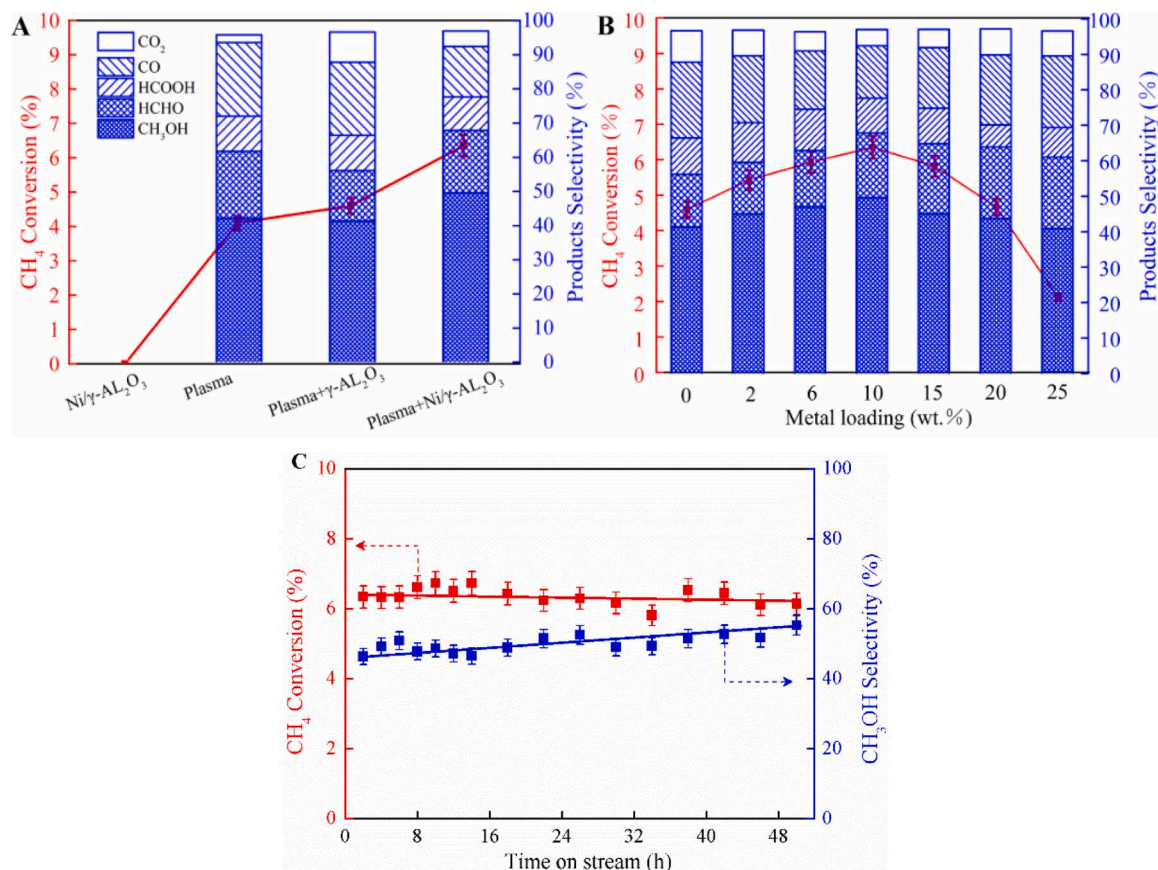


Fig. 1. Experimental results of SOMTM. (A). CH₄ conversion and products selectivity, using only NiO/γ-Al₂O₃ catalyst, only plasma, plasma with γ-Al₂O₃ beads, and plasma with (10 wt.%) NiO/γ-Al₂O₃ catalyst (400 mL/min CH₄, 200 mL/min O₂, 85 °C circulating water, 1.25 g NiO/γ-Al₂O₃ catalyst, 30 W discharge power and 0.375 s residence time). (B). Effect of Ni loading on CH₄ conversion and products selectivity, for plasma with NiO/γ-Al₂O₃ catalyst. (C). Stability test of the (10 wt.%) NiO/γ-Al₂O₃ catalyst in CH₄/O₂ NTP during 50 h continuous operation.

distribution is shown in Figs. S7 and S8, and the total selectivity of liquid oxygenates reaches 80.7 %. This striking result is again attributed to the short residence time, as illustrated by the modeling below.

Furthermore, we studied NiO/γ-Al₂O₃ catalysts with varied loading (Fig. 1B). The highest CH₄ conversion and CH₃OH selectivity were both achieved at 10 wt.% loading. Moreover, we operated the CH₄/O₂ NTP with 10 wt.% NiO/γ-Al₂O₃ catalyst continuously for 50 h, and the CH₄ conversion and CH₃OH selectivity remained stable (Fig. 1C), indicating

the excellent catalytic stability of the NiO/γ-Al₂O₃ catalyst in CH₄/O₂ NTP for CH₃OH production. The results obtained in this paper have been compared with those in literature. As shown in Fig. 2A, the CH₃OH productivity (27.3 mmol g_{cat}⁻¹ h⁻¹) calculated by formula (1) of the SI is two orders of magnitude higher than the best results obtained through stoichiometric chemical looping using O₂ as the oxidant [20,38]. As shown in Fig. 2B, the CH₃OH selectivity is higher than the best results obtained through plasma catalysis, using various catalysts, albeit at a

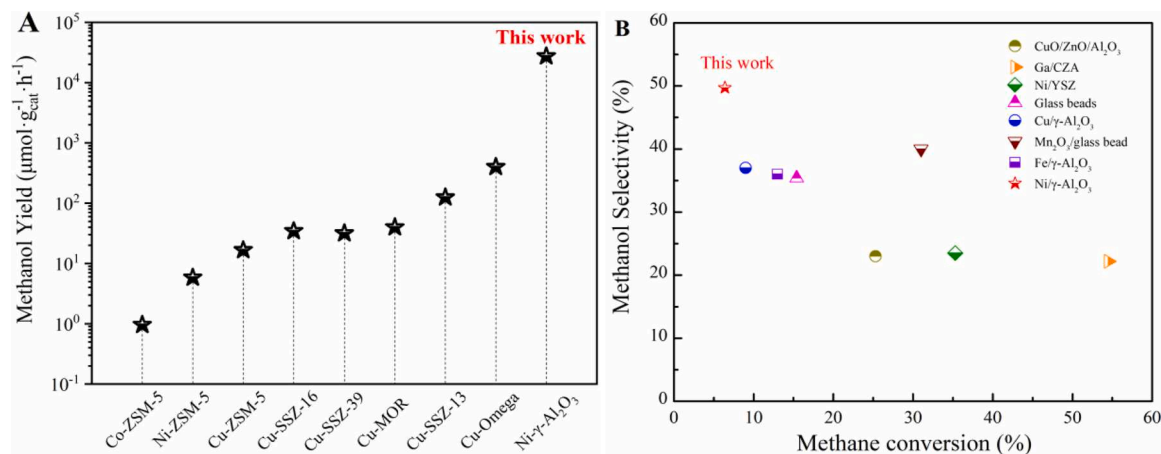


Fig. 2. Comparison of this work with literature results. A: CH₃OH productivity by stoichiometric chemical looping using O₂ as the oxidant, for different catalyst materials (calculated based on the results adapted from references [20] and [38]); B: CH₃OH selectivity by plasma catalysis using O₂ as the oxidant (adapted from reference [30–32]).

lower CH₄ conversion [30–32].

The hydrogen-based products selectivity is shown in Fig. S9. The selectivity of CH₃OH is almost 50 % in the case of “plasma + NiO/ γ -Al₂O₃ catalyst, i.e., over 18 % higher than in the case of plasma or plasma + γ -Al₂O₃ beads. The H₂ and H₂O selectivities reach 5.6 % and 29.1 %, respectively, while the selectivities of HCHO and HCOOH are around 9 % and 4.9 %, respectively, in the case of “plasma + NiO/ γ -Al₂O₃ catalyst (10 wt.% loading).

Energy efficiency is a key performance indicator for plasma-catalytic SOMTM. We defined the energy efficiency for CH₃OH formation by formula (7), in which the plasma power was calculated through mathematical integration using the waveform of discharge voltage (Fig. S10) and discharge current (Fig. S11). As illustrated by Fig. S12, the energy efficiency in the plasma-only case is 0.76 mol/kWh; it rises slightly to 0.95 mol/kWh with γ -Al₂O₃, but with NiO/ γ -Al₂O₃, it rises dramatically to 1.4 mol/kWh. Thus, while the CH₄ conversion and CH₃OH selectivity only increase by 2.3 % and 7.5 %, respectively, in case of plasma catalysis compared to plasma alone, the energy efficiency rises by 84 %. Furthermore, the produced methanol with high concentration (1.3 mol/L) in liquid can be condensed in the online cold-trap, without further methanol extraction using a solvent or steam, which can avoid a step-wise process on heterogeneous catalysis. This continuous operation condition under low temperature and atmosphere pressure exhibited the great potential for plasma-catalytic SOMTM by CH₄/O₂ NTP.

3.2. Chemical kinetics modelling of CH₄/O₂ DBD plasma

As mentioned above, in plasma alone, we achieved 42 % CH₃OH selectivity (Fig. 1A), which is much better than most results in literature [28–36]. To explain this result, we performed chemical kinetics modelling of CH₄/O₂ DBD plasma using ZDPlaskin [39]. Details about the modelling, the species (Table S2) and reactions (Tables S3–S5) in the model, are presented in SI.

The lines in Fig. 3 depict the calculated products selectivity as function of residence time, derived from the densities of the species in the plasma (Fig. S13). Initially, the calculated CH₃OH selectivity is extremely high (~78 %), but it decreases gradually upon increasing residence time, until about 30 % for a residence time of 1.2 s. HCHO exhibits a similar evolution (but with maximum selectivity around 20 %), while CO, HCOOH and CO₂ exhibit the opposite trend. To verify the modelling, we performed experiments at varying residence time (symbols in Fig. 3). The experimental selectivities of CH₃OH, HCHO, CO and CO₂ agree reasonably well with the modelling results (similar trends),

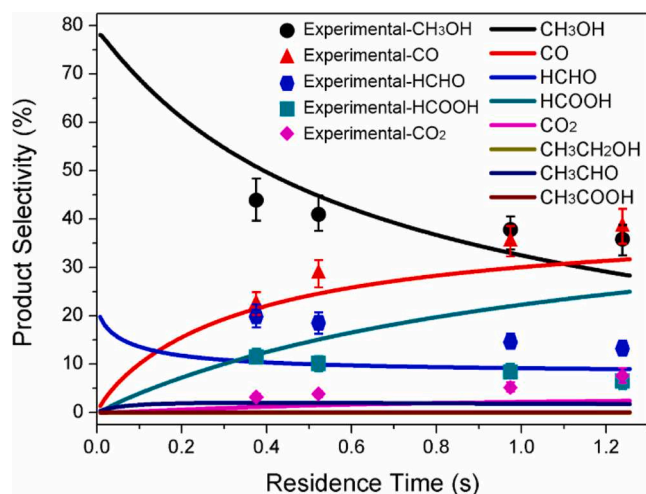


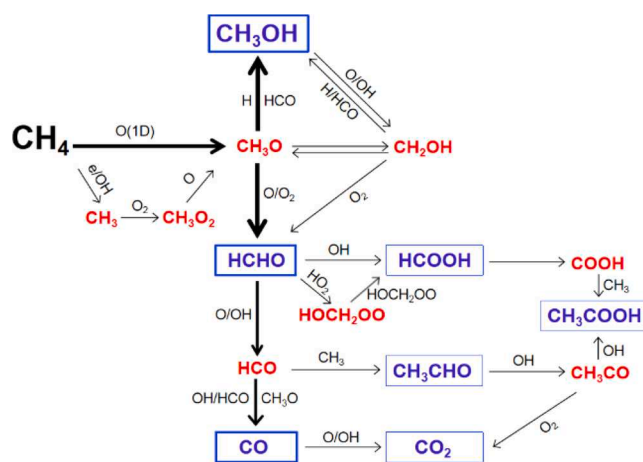
Fig. 3. Products selectivity in CH₄/O₂ plasma, obtained by chemical kinetics modeling (lines) and experiments (symbols) as function of residence time, for the same conditions as in Fig. 1.

indicating that the model provides a realistic picture of the formation of these products in the CH₄/O₂ plasma. For HCOOH, however, the agreement is not yet satisfying, suggesting that important production or loss processes for HCOOH might be missing in the model, or that their rate coefficients are not correct, but we can only rely on the input data (chemical reactions and corresponding rate coefficients) available in literature, and we don't want to tune the model to fit it to the experiments without scientific basis. However, it means that our model cannot yet be used to predict the reaction pathways for HCOOH, but we can use it for the other possible reaction pathways in the CH₄/O₂ plasma. As shown in Scheme 1, CH₃OH is mainly produced from CH₃O species through the reactions CH₃O + H + M → CH₃OH + M and CH₃O + HCO → CH₃OH + CO.

3.3. NiO/ γ -Al₂O₃ Catalysts characterization

In spite of the high CH₃OH selectivity at short residence time, the CH₄ conversion is quite low (4.1 %), caused by the high space velocity. However, as shown in Fig. 1, the Ni catalyst (with 10 wt. % loading) enhances both the CH₄ conversion and CH₃OH selectivity. It is very interested that both CH₄ conversion and CH₃OH selectivity synchronously reached the highest value at 10 wt.% loading, since generally CH₃OH selectivity decreases with the increase of CH₄ conversion. To reveal the unique role of the Ni-based catalysts, we characterized them by XRD, HAADF-STEM, H₂-TPR, XPS, HRTEM, XRF and N₂ physisorption.

The XRD result (Fig. 4A) reveals no evident NiO peak for Ni loadings below 10 wt.%, indicating the high dispersion of the NiO particles on γ -Al₂O₃. However, a group of NiO diffraction peaks gradually appears upon increasing metal loading, showing the formation of larger NiO particles. The NiO crystal size is estimated by the Debye – Scherrer equation, presented in Table S6. It is observed that NiO particles on NiO/ γ -Al₂O₃ with Ni loading from 15 to 25 % are in the range of 10.3–22.1 nm. In addition, the adsorption-desorption isotherm and pore size distribution curve of the catalysts are shown in Fig. S14, and the corresponding surface values are presented in Table S6. Clearly, surface area of NiO/ γ -Al₂O₃ catalysts gradually declined with the increasing of Ni loading, and γ -Al₂O₃ support shows the highest surface area (216.5 m²/g). By correlating the surface area (Table S6) with the reaction performance (Fig. 1), it can be concluded that surface area is not the key factor



Scheme 1. Reaction pathways for the formation of CH₃OH and other oxygenates in the CH₄/O₂ plasma, predicted by chemical kinetics modelling (ZDPlaskin). Red color indicates reaction intermediates and blue color with rectangles means stable products. The size of the products is approximately proportional to their selectivity and the thickness of the arrow lines is proportional to the net rate of that reaction. (For interpretation of the references to colour in this figure legend, the reader is referred to the web version of this article).

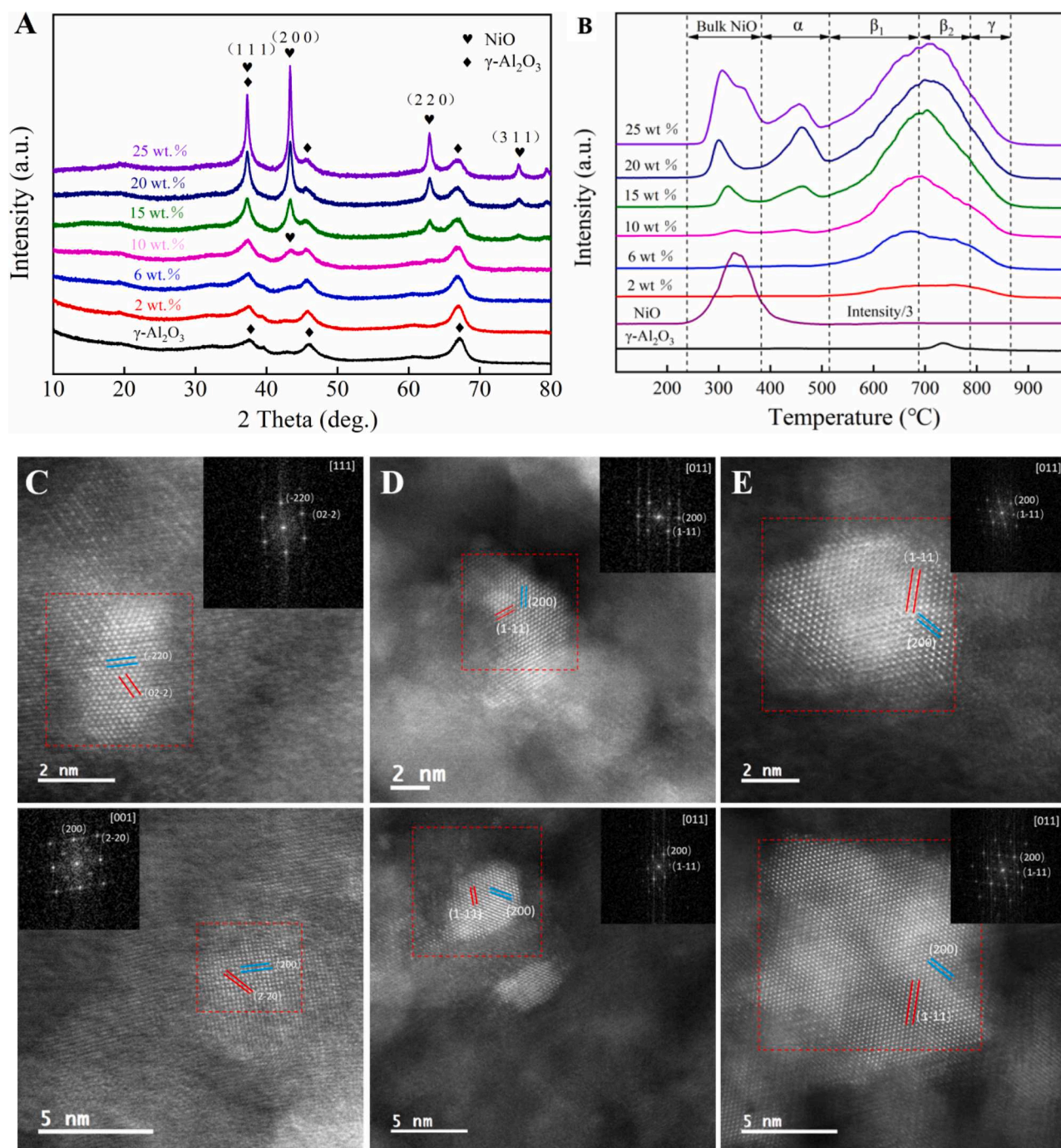


Fig. 4. Characterization results of the NiO/ γ -Al₂O₃ catalysts with varying loadings. (A) XRD patterns; (B) H₂-TPR profiles; (C) HAADF-STEM image of NiO/ γ -Al₂O₃ catalyst with 2 wt.% loading; (D) HAADF-STEM image of NiO/ γ -Al₂O₃ catalyst with 10 wt.% loading; (E) HAADF-STEM image of NiO/ γ -Al₂O₃ catalyst with 25 wt.% loading.

in determining catalytic performance of NiO/ γ -Al₂O₃ catalysts in DOMTM.

Fig. 4C–E shows HAADF-STEM images of 2 wt.% NiO/ γ -Al₂O₃, 10 wt.% NiO/ γ -Al₂O₃ and 25 wt.% NiO/ γ -Al₂O₃ catalysts, respectively. Clearly, the NiO particle size in 2 wt.% NiO/ γ -Al₂O₃ and 10 wt.% NiO/ γ -Al₂O₃ is very small (< 5 nm), but the size in 25 wt.% NiO/ γ -Al₂O₃ is bigger (> 10 nm). Fig. S15 shows the HAADF-STEM mapping results of 6 wt.% NiO/ γ -Al₂O₃, 15 wt.% NiO/ γ -Al₂O₃ and 20 wt.% NiO/ γ -Al₂O₃. It can be seen that NiO was uniformly dispersed in 6 wt.% NiO/ γ -Al₂O₃. In 15 wt.% NiO/ γ -Al₂O₃ and 20 wt.% NiO/ γ -Al₂O₃, however, NiO particles with size more than 10 nm can be clearly observed. HRTEM images

(Fig. S16) show similar results. These morphology results indicate that NiO was highly dispersed on the surface of γ -Al₂O₃ with low loading (2, 6 and 10), and also demonstrate the larger NiO particles at higher Ni loadings. Furthermore, a lattice space of 0.21 nm and 0.24 nm, attributed to the (200) and (111) planes, was observed by HRTEM (Fig. S17), and similar results were also obtained from fast Fourier transformation (FFT) of NiO particles in the HAADF-STEM images (Fig. 4C–E), consistent with the XRD results (Fig. 4A).

The H₂-TPR profiles of the NiO/ γ -Al₂O₃ catalysts are shown in Fig. 4B (NiO was used as a reference), and quantitative TPR results are presented in Fig. S18 and Table S7. Five reducible peaks, at 280–350 °C,

390–510 °C, 510–690 °C, 690–790 °C and 790–840 °C, were detected, attributed to the reduction of five kinds of NiO species, i.e., bulk NiO (without interaction with Al₂O₃), α -type NiO (weak oxide-support interaction, WOSI), β_1 -type NiO (strong oxide-support interaction (SOSI), with Ni abundant on surface), β_2 -type NiO (SOSI, with Al abundant on surface) and γ -type NiO (nickel aluminum spinel; strongest

interaction with Al₂O₃), respectively [40–42]. Obviously, β_1 , β_2 and γ -type NiO are present in all NiO/ γ -Al₂O₃ catalysts. On the other hand, α -type and bulk NiO only appear for Ni loadings above 10 wt.%. This corresponds to the XRD results, where obvious diffraction peaks of NiO (larger particles) were formed at high loading (15 %, 20 % and 25 %). This is also consistent with the morphology results, where bigger NiO

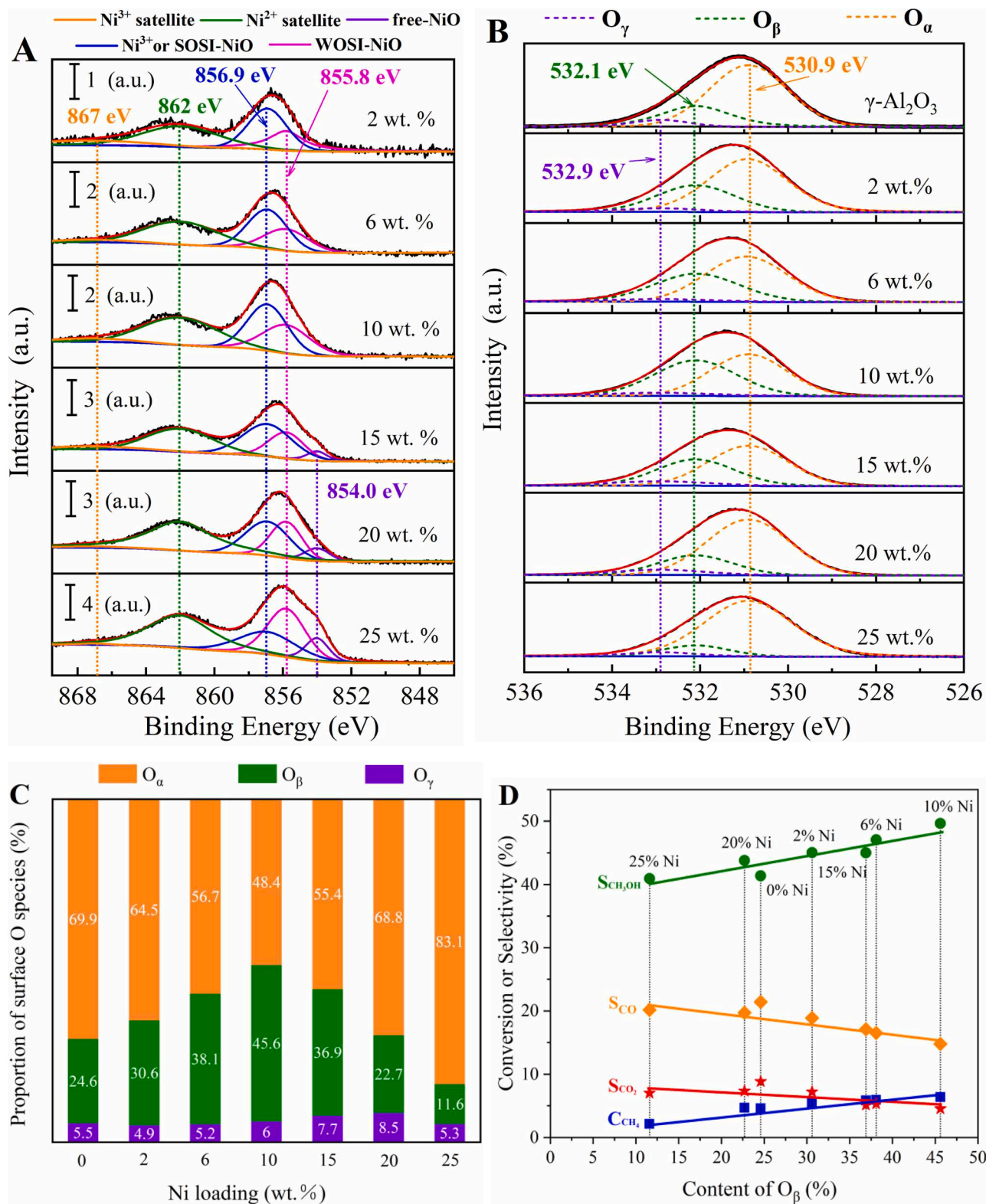


Fig. 5. XPS results of the NiO/ γ -Al₂O₃ catalysts with varying loadings. (A) Ni 2p region; (B) O 1s region; (C) Proportion of oxygen species for varied loading of Ni on γ -Al₂O₃; (D) Linear relationship between content of chemisorbed oxygen species (O_β) and reaction performance.

particles have been observed at high loading (15 %, 20 % and 25 %).

The XPS profiles of the Ni 2p and O 1s of the NiO/ γ -Al₂O₃ catalysts with various Ni loadings are shown in Fig. 5A and B, respectively (Al 2p results are shown in Fig. S19). For Ni 2p, three peaks, corresponding to a binding energy at 854.0, 855.8 and 856.9 eV, have been detected. The low binding energy peak (854.0 eV) is assigned to free-NiO species (big NiO particles) [43,44]. The moderate binding energy peak (855.8 eV) is usually attributed to NiO species with WOSI [45]. The high binding energy peak (856.9 eV), however, generally results from NiO species with SOSI or Ni³⁺ species [44,46]. On the other hand, the intensity of the satellite peak of Ni³⁺ is extremely low (it can nearly be ignored), which means that there is few Ni³⁺ species on the catalyst surface, and thus the peak of binding energy at 856.9 eV is mainly attributed to NiO species with SOSI.

Furthermore, at low loading (2, 6 and 10 wt.%), Ni mainly exists as NiO species with SOSI, since the peak of binding energy at 856.9 eV dominates the whole Ni 2p peak. On the other hand, at higher loading (15, 20 and 25 wt.%), Ni mainly exists as NiO species with WOSI and free-NiO, because the peak at 854.0 eV appears and the contribution of the peak at 855.8 eV increases. The surface information obtained by XPS analysis is consistent with the above XRD, TEM and H₂-TPR results.

The O 1s spectra of NiO/ γ -Al₂O₃ catalysts presented in Fig. 5B can be fitted into three peaks, corresponding to the lattice oxygen of metal oxide (O_α), chemisorbed oxygen (O_β), and adsorbed water or OH species (O_γ), with binding energy at 530.9 eV, 532.1 eV and 532.9 eV, respectively [47,48].

As shown in Fig. 5C, upon increasing Ni loading from 2 to 10 wt.%, the proportion of O_β species on the catalyst surface rises, and reaches the

highest value (45.6 %) at 10 wt.% loading, and then it decreases. Interestingly, the variation trend of Ni 2p peak of SOSI NiO (Fig. 5A) is synchronous with O 1s of O_β species, which means that the chemisorbed oxygen, i.e., O_β species, mainly comes from the SOSI NiO. Lattice oxygen, i.e., O_α species, are undoubtedly from crystals, i.e., γ -Al₂O₃ support, free-NiO particles, and big NiO particles with WOSI. Upon increasing Ni loading, the proportion of O_α species, however, firstly decreases and then increases, and the lowest proportion was found at 10 wt.% loading, which means that the defects on the surface of 10 wt.% NiO/ γ -Al₂O₃ catalysts is much more than those of the other catalysts. The defects have been created by SOSI, and usually, the created defects on metal oxide are not stable. In an oxidizing atmosphere, they tend to combine with oxygen to form chemisorbed oxygen, i.e., O_β species. That is, NiO with SOSI leads to surface chemisorbed oxygen species.

Fig. 5D presents the reaction performance (CH₄ conversion, CH₃OH selectivity, CO and CO₂ selectivity) as a function of O_β content on the catalyst surface. Interestingly, with increasing O_β species content, both CH₄ conversion and CH₃OH selectivity rise linearly, while both CO and CO₂ selectivity decrease linearly. Therefore, it can be reasonably inferred that chemisorbed oxygen, i.e., O_β species, are the real active sites for CH₄ to CH₃OH conversion in this study. In contrast, lattice oxygen species, i.e., O_α, may be the sites leading to deep oxidation to produce CO and CO₂ (Fig. S20).

TG-MS results (Fig. S21) shows very limited carbon deposition. In addition, the fresh and spent NiO/ γ -Al₂O₃ (10 wt.%) catalysts were compared by XRD (Fig. S22), H₂-TPR (Fig. S23) and XPS (Fig. S24), and no evident changes were observed. These results demonstrate the excellent catalytic stability of NiO/ γ -Al₂O₃ catalyst in CH₄/O₂ NTP for

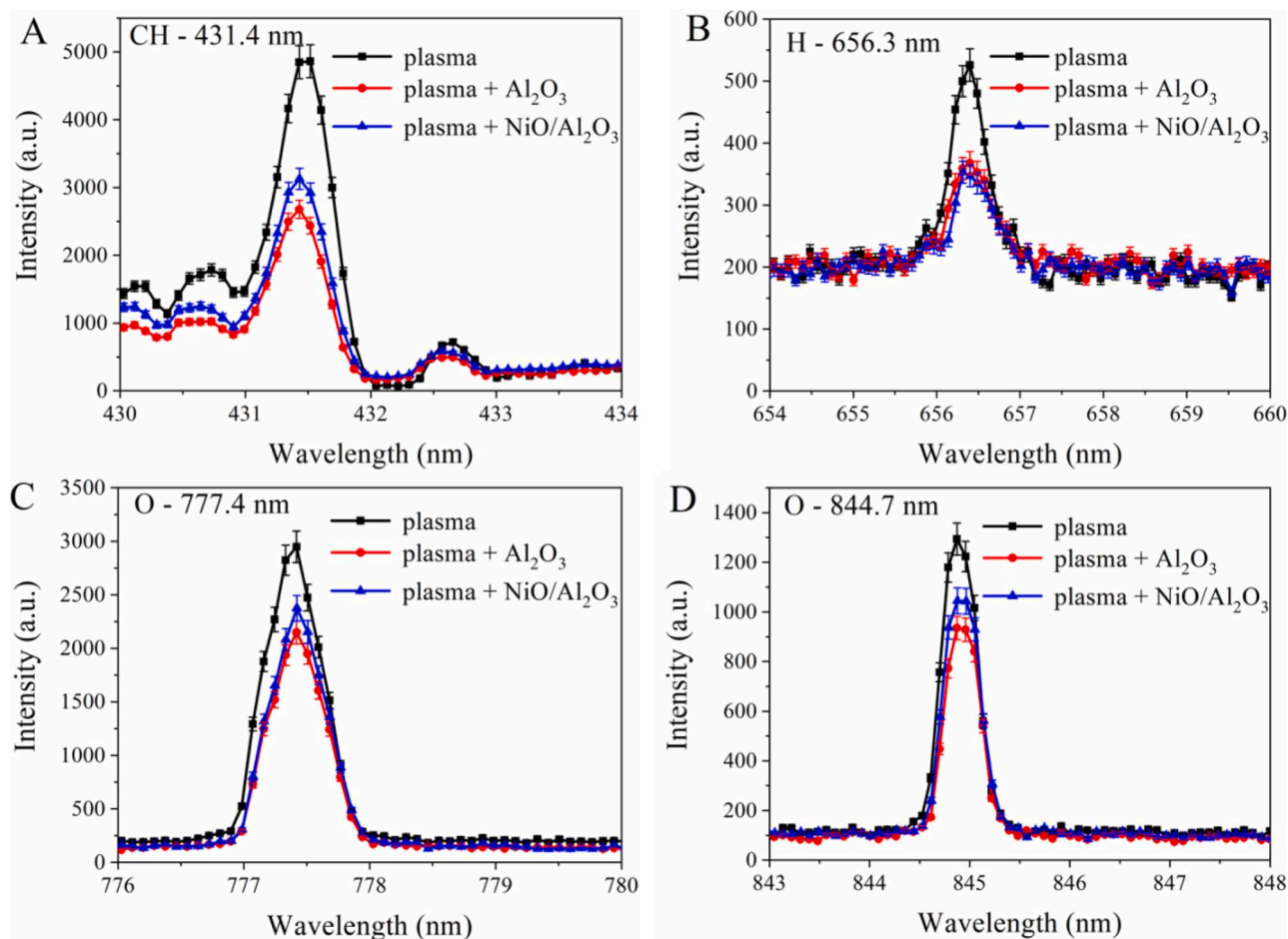


Fig. 6. OES intensities of (A) CH (431.4 nm), (B) H (656.3 nm), (C) O (777.4 nm) and (D) O (844.7 nm), in the case of plasma alone, plasma + γ -Al₂O₃ beads, and plasma +(10 wt%) NiO/ γ -Al₂O₃ catalyst, for the same conditions as in Fig. 1.

CH₃OH production. Some other information of the NiO/ γ -Al₂O₃ catalysts, i.e., the real loading, surface area and porosity, is shown in Table S6.

3.4. NTP diagnostics and reaction mechanism

OES diagnostics were employed to reveal some of the important plasma species playing a role in CH₄/O₂ NTP for CH₃OH synthesis. As shown in Figs. 6 and S25, CH (431.4 nm), H (656.3 nm) and O (777.4 nm and 844.7 nm) were directly identified, demonstrating the existence of CH, H and O species in the plasma. However, also other reactive species are present in the plasma, which cannot be observed by OES.

Morgan and Erwin stated that CH₄ can be decomposed into CH₃, CH₂ and CH neutral fragments [49,50]. Based on a 1D fluid model, De Bie et al. predicted a probability of producing CH₃, CH₂ and CH radicals in CH₄ DBD plasma of 79 %, 15 % and 5 %, respectively [51]. A similar trend was predicted in a CH₄/O₂ DBD plasma, again by a 1D fluid model [52]. Therefore, we can assume that CH₃ is more abundant than CH₂ and CH in the CH₄/O₂ NTP. The reason why CH₃ was not detected by OES is because its emission lines appear in the infrared region, which is out of the wavelength range of our OES measurements. For the oxidative species, the lines at 777.4 nm and 844.7 nm were detected by OES, attributed to deexcitation of O (3p⁵P) and O (3p³P) atoms, respectively [53]. However, the pathways for activation of O₂ through inelastic collisions with energetic electrons, as listed in Fig. S26, indicate that the generation of O (¹D) is easier than the generation of O (3p⁵P) and O (3p³P) [54,55]. The reason why we did not detect O (¹D) by OES is that it is a metastable species with long lifetime, which dissipates its internal energy by chemical reactions, instead of deexcitation. Therefore, there will be abundant CH₃ radicals and O (¹D) atoms in the CH₄/O₂ NTP, which confirms the reaction pathway in Scheme 1, triggered by O (¹D) and CH₃. The above OES results show that, in CH₄/O₂ plasma, there are abundant CH₃, O (¹D) and H radical species.

Tang et al. predicted that CH₃OH synthesis usually proceeds through the Langmuir-Hinshelwood (L-H) mechanism in thermal catalysis [56]. In plasma catalysis, however, CH₃OH might be formed by both Eley-Rideal (E-R) and L-H mechanisms [32,57,58]. On the NiO/ γ -Al₂O₃ (10 wt.%) catalyst surface, chemisorbed oxygen is abundant, which has been demonstrated by our XPS results. On the other hand, in the gas-phase, CH₃ and O radicals are also abundant, as proven by our OES results. Therefore, it can be reasonably assumed that CH₃O species can be formed, not only through radical reactions in gas-phase (proven by our modelling results in Scheme 1), i.e., CH₃O_(g), but also through reaction between CH₃ in gas phase and chemisorbed oxygen on the catalyst surface, i.e., CH₃O_(ad). That is, due to the reactivity of the CH₃ radicals caused by their internal energy, the formation of CH₃O species through E-R reaction between CH₃ radicals and chemisorbed oxygen will be very fast. Subsequently, the formed CH₃O species may result in the generation of CH₃OH through recombination with a H atom generated by CH₄/O₂ plasma (E-R reaction) [32]. Therefore, the reason why the NiO/ γ -Al₂O₃ (10 wt.%) catalyst shows the best CH₄ conversion may be that it contains the highest content of chemisorbed oxygen. In the case of plasma-catalytic CH₄ to CH₃OH conversion, the formation and desorption of one CH₃OH molecule will consume one O _{β} species (as O _{β} is the real active site). In conventional heterogeneous catalysis, this may lead to a continuous decrease of the O _{β} content at the catalyst surface, and thus the reaction performance would decline since the catalytic cycle cannot be completed. However, in the case of plasma catalysis, O₂ is activated by the plasma into O atoms (either in ground or excited states, e.g., ¹D), which are very reactive, and easily interact with the catalyst surface. So, we believe that these O atoms are capable of interacting with the catalyst surface to rapidly form O _{β} species, which compensates for the consumption of O _{β} species producing CH₃OH. In other words, the plasma-generated reactive oxygen species enable the fast catalytic cycle for CH₄ oxidation to CH₃OH.

The produced CH₃OH molecule usually strongly adsorbs on the

catalyst surface, making desorption difficult and resulting in deep oxidation, which is the key factor inhibiting the CH₃OH selectivity, and it is the issue many researchers are concerning. As reported by Lustenberg, water molecules can be activated by Ni/CeO₂ catalyst with strong metal-support interactions, and then the activated H₂O molecule can promote CH₃OH desorption [37]. In addition, Water molecular can act as a site blocker, which can preferentially occupy the active Ce sites at the CeO₂-Cu₂O catalyst interface and hinder methane overoxidation to CO and CO₂, meanwhile, it can also act as an active center where the active *OH was produced at interfacial Ce sites to promote methanol synthesis [15]. In the stepwise process using copper-exchanged zeolites, H₂O molecule also plays an essential role in promoting CH₃OH formation and desorption [59,60]. Chemical kinetics modeling result (Fig. S13) shows that H₂O molecules are abundant in the CH₄/O₂ NTP. The measured products selectivity based on hydrogen (Fig. S9) shows that the selectivity of H₂O reached 29.1 %, demonstrating that H₂O molecules are abundant in CH₄/O₂ NTP. As demonstrated by our XPS results (Fig. 5), caused by SOSI, the defects are also abundant at the interface between NiO particles and γ -Al₂O₃ support, especially for the NiO/ γ -Al₂O₃ catalyst with 10 wt.% loading. Therefore, we believe that the H₂O molecule produced by CH₄/O₂ plasma can also be activated by NiO/ γ -Al₂O₃ catalyst with SOSI, and the activated H₂O molecule may promote desorption of CH₃OH, which may be the reason why the NiO/ γ -Al₂O₃ (10 wt.%) catalyst shows the best CH₃OH selectivity. The role of plasma and Ni-based catalyst in SOMTM has been summarized in Scheme 2.

4. Conclusion

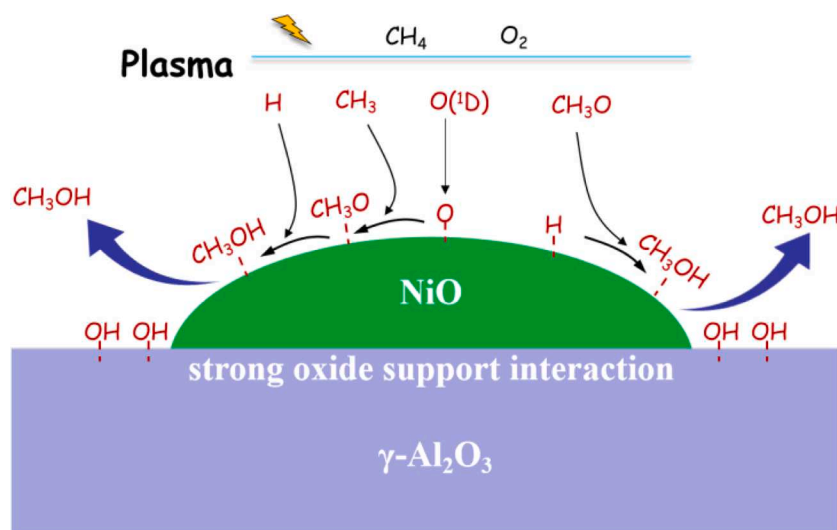
We demonstrated the selective oxidation of methane to methanol (SOMTM) in CH₄/O₂ plasma, promoted by Ni-based catalysts, with excellent catalytic stability. 76 % liquid oxygenates selectivity with 42 % CH₃OH selectivity are achieved in plasma alone, and the selectivities are further enhanced to 81 % and 50 %, respectively, when adding NiO/ γ -Al₂O₃ catalyst with 10 wt.% loading. The energy efficiency by plasma catalysis is improved with 84 % comparing to plasma alone (from 0.76 to 1.4 mol/kWh).

In addition, chemical kinetics modelling shows that within the plasma, CH₃OH is mainly produced through radical reactions, i.e., CH₄ + O(¹D) → CH₃O + H, followed by CH₃O + H + M → CH₃OH + M and CH₃O + HCO → CH₃OH + CO. The catalyst characterization shows that the further improvement in CH₃OH production by plasma catalysis is attributed to the highly dispersed NiO phase with SOSI. This causes an improvement of chemisorbed oxygen species, which catch CH₃ radicals from the plasma to form CH₃O_{ad} species. The latter can form CH₃OH through the ER reaction with H atoms from the plasma. Furthermore, H₂O molecules produced by CH₄/O₂ plasma may also be activated by NiO/ γ -Al₂O₃ catalyst with SOSI, and the activated H₂O molecules may promote desorption of CH₃OH. The highest content of chemisorbed oxygen species can explain why the NiO/ γ -Al₂O₃ catalyst with 10 wt.% loading shows both the best CH₄ conversion and the best CH₃OH selectivity.

Further work will be focused on enhancing the plasma-catalyst synergy through modifying the NiO/ γ -Al₂O₃ catalyst by electronic promoters (multi-component catalysts), which should allow to enhance the adsorption capacity towards reaction intermediates (CH₃O, etc.) and the desorption of favorable target products, aiming to further improve the CH₄ conversion and CH₃OH selectivity.

Author contributions

The manuscript was written through contributions of all authors. All authors have given approval to the final version of the manuscript. Notes The authors declare no competing financial interest.



Scheme 2. Suggested reaction pathways of CH_3OH formation in CH_4/O_2 plasma promoted by $\text{NiO}/\gamma\text{-Al}_2\text{O}_3$ catalyst with SOSI (see text).

CRediT authorship contribution statement

Yanhui Yi: Conceptualization, Validation, Formal analysis, Resources, Data curation, Writing - original draft, Writing - review & editing, Supervision, Funding acquisition. **Shangkun Li:** Conceptualization, Validation, Formal analysis, Resources, Data curation, Writing - original draft, Writing - review & editing. **Zhaolun Cui:** Validation, Formal analysis, Data curation, Writing - original draft. **Yingzi Hao:** Validation, Formal analysis, Data curation, Writing - original draft. **Yang Zhang:** Resources, Data curation. **Li Wang:** Validation, Formal analysis, Resources. **Pei Liu:** Resources, Data curation. **Xin Tu:** Resources, Data curation. **Xianming Xu:** Resources, Data curation. **Hongchen Guo:** Resources, Data curation. **Annemie Bogaerts:** Formal analysis, Resources, Data curation, Writing - original draft, Writing - review & editing, Supervision, Funding acquisition.

Declaration of Competing Interest

The authors declare that they have no known competing financial interests or personal relationships that could have appeared to influence the work reported in this paper.

Acknowledgements

We acknowledge financial support from the PetroChina Innovation Foundation [grant ID: 2018D-5007-0501], the Young Star Project of Dalian Science and Technology Bureau [grant ID: 2019RQ042], the National Natural Science Foundation of China [grant ID: 21503032] and the TOP research project of the Research Fund of the University of Antwerp [grant ID: 32249].

Appendix A. Supplementary data

Supplementary material related to this article can be found, in the online version, at doi:<https://doi.org/10.1016/j.apcatb.2021.120384>.

References

- A. Caballero, P. Perez, Methane as raw material in synthetic chemistry the final frontier, *Chem. Soc. Rev.* 42 (2013) 8809–8820.
- J. Xie, R. Jin, A. Li, Y. Bi, Q. Ruan, Y. Deng, Y. Zhang, S. Yao, G. Sankar, D. Ma, J. Tang, Highly selective oxidation of methane to methanol at ambient conditions by titanium dioxide-supported iron species, *Nat. Catal.* 1 (2018) 889–896.
- X. Meng, X. Cui, N.P. Rajan, L. Yu, D. Deng, X. Bao, Direct methane conversion under mild condition by thermo-, electro-, or photocatalysis, *Chemistry* 5 (2019) 1–30.
- R.A. Periana, D.J. Taube, E.R. Evitt, D.G. Loffler, P.R. Wentreck, G. Voss, T. Masuda, A. Mercury-Catalyzed, High-yield system for the oxidation of methane to methanol, *Science* 259 (1993) 340–343.
- R.A. Periana, D.J. Taube, S. Gamble, H. Taube, T. Satoh, H. Fujii, Platinum catalysts for the high-yield oxidation of methane to a methanol derivative, *Science* 280 (1998) 560–564.
- M. Muehlhofer, T. Strassner, W.A. Herrmann, New catalyst systems for the catalytic conversion of methane into methanol, *Angew. Chem. Int. Ed.* 41 (2002) 1745–1747.
- M.V. Parfenov, E.V. Starokon, L.V. Pirutko, G.I. Panov, Quasicatalytic and catalytic oxidation of methane to methanol by nitrous oxide over FeZSM-5 zeolite, *J. Catal.* 318 (2014) 14–21.
- C. Hammond, M.M. Forde, M.H. Ab Rahim, A. Thetford, Q. He, R.L. Jenkins, N. Dimitratos, J.A. Lopez-Sanchez, N.F. Dummer, D.M. Murphy, A.F. Carley, S. H. Taylor, D.J. Willock, E.E. Stangland, J. Kang, H. Hagen, C.J. Kiely, G. J. Hutchings, Direct catalytic conversion of methane to methanol in an aqueous medium by using copper-promoted Fe-ZSM-5, *Angew. Chem. Int. Ed.* 51 (2012) 5129–5133.
- M.H. Groothaert, P.J. Smeets, B.F. Sels, P.A. Jacobs, R.A. Schoonheydt, Selective oxidation of methane by the bis(μ -oxo)copper core stabilized on ZSM-5 and mordenite zeolites, *J. Am. Chem. Soc.* 127 (2005) 1394–1395.
- S. Grundner, M.A. Markovits, G. Li, M. Tromp, E.A. Pidko, E.J. Hensen, A. Jentys, M. Sanchez-Sanchez, J.A. Lercher, Single-site trinuclear copper oxygen clusters in mordenite for selective conversion of methane to methanol, *Nat. Comm.* 6 (2015) 7546.
- D.K. Pappas, E. Borfecchia, M. Dyballa, I.A. Pankin, K.A. Lomachenko, A. Martini, M. Signorile, S. Teketel, B. Arstad, G. Berlier, C. Lamberti, S. Bordiga, U. Olsbye, K. P. Lillerud, S. Svelle, P. Beato, Methane to methanol: structure-activity relationships for Cu-CHA, *J. Am. Chem. Soc.* 139 (2017) 14961–14975.
- N. Agarwal, S. Freakley, R.U. McVicker, S.M. Althabban, N. Dimitratos, Q. He, D. J. Morgan, R.L. Jenkins, D.J. Willock, S.H. Taylor, C.J. Kiely, G.J. Hutchings, Aqueous Au-Pd colloids catalyze selective CH_4 oxidation to CH_3OH with O_2 under mild conditions, *Science* 358 (2017) 223–227.
- J. Shan, M. Li, L.F. Allard, S. Lee, M. Flytzani-Stephanopoulos, Mild oxidation of methane to methanol or acetic acid on supported isolated rhodium catalysts, *Nature* 551 (2017) 605–608.
- Z. Zuo, P.J. Ramirez, S.D. Senanayake, P. Liu, J.A. Rodriguez, Low-temperature conversion of methane to methanol on $\text{CeO}_2/\text{Cu}_2\text{O}$ catalysts: water controlled activation of the C-H bond, *J. Am. Chem. Soc.* 138 (2016) 13810–13813.
- Z. Liu, E. Huang, I. Orozco, W. Liao, R.M. Palomino, N. Rui, T. Duchon, S. Nemsak, D.C. Grinter, M. Mahapatra, P. Liu, J.A. Rodriguez, S.D. Senanayake, Water-promoted interfacial pathways in methane oxidation to methanol on a $\text{CeO}_2\text{-Cu}_2\text{O}$ catalyst, *Science* 368 (2020) 513–517.
- Z. Jin, L. Wang, E. Zuidema, K. Mondal, M. Zhang, J. Zhang, C. Wang, X. Meng, H. Yang, C. Mesters, F. Xiao, H_2O_2 Hydrophobic zeolite modification for in situ peroxide formation in methane oxidation to methanol, *Science* 367 (2020) 193–197.
- M. Ravi, M. Ranocchiaro, J.A. van Bokhoven, The direct catalytic oxidation of methane to methanol—a critical assessment, *Angew. Chem. Int. Ed.* 56 (2017) 16464–16483.
- X. Cui, H. Li, Y. Wang, Y. Hu, L. Hua, H. Li, X. Han, Q. Liu, F. Yang, L. He, X. Chen, Q. Li, J. Xiao, D. Deng, X. Bao, Room-temperature methane conversion by graphene-confined single iron atoms, *Chemistry* 4 (2018) 1902–1910.
- P. Tomkins, M. Ranocchiaro, J.A. van Bokhoven, Direct conversion of methane to methanol under mild conditions over Cu-Zeolites and beyond, *Acc. Chem. Res.* 50 (2017) 418–425.

- [20] M.H. Mahyuddin, Y. Shiota, K. Yoshizawa, Methane selective oxidation to methanol by metal-exchanged zeolites: a review of active sites and their reactivity, *Catal. Sci. Technol.* 9 (2019) 1744–1768.
- [21] J.P. Lange, V.L. Sushkevich, A.J. Knorpp, J.A. van Bokhoven, Methane-to-methanol via chemical looping economic potential and guidance for future research, *Ind. Eng. Chem. Res.* 58 (2019) 8674–8680.
- [22] L. Wang, Y. Yi, H. Guo, X. Tu, Atmospheric pressure and room temperature synthesis of methanol through plasma-catalytic hydrogenation of CO₂, *ACS Catal.* 8 (2017) 90–100.
- [23] J. Sentek, K. Krawczyk, M. Mlotek, M. Kalczyńska, T. Kroker, T. Kolb, A. Schenk, K.-H. Gericke, K. Schmidt-Szałowski, Plasma-catalytic methane conversion with carbon dioxide in dielectric barrier discharges, *Appl. Catal. B: Environ.* 94 (2010) 19–26.
- [24] D. Li, V. Rohani, F. Fabry, A. Parakkulam Ramaswamy, M. Sennour, L. Fulcheri, Direct conversion of CO₂ and CH₄ into liquid chemicals by plasma-catalysis, *Appl. Catal. B: Environ.* 261 (2020), 118228.
- [25] L. Wang, Y. Yi, C. Wu, H. Guo, X. Tu, One-Step Reforming of CO₂ and CH₄ into high-value liquid chemicals and fuels at room temperature by plasma-driven Catalysis, *Angew. Chem. Int. Ed.* 56 (2017) 13679–13683.
- [26] C.E. Stere, J.A. Anderson, S. Chansai, J.J. Delgado, A. Goguet, W.G. Graham, C. Hardacre, S.F. Rebecca Taylor, X. Tu, Z. Wang, H. Yang, Non-thermal plasma activation of gold-based catalysts for low-temperature water-gas shift catalysis, *Angew. Chem. Int. Ed.* 56 (2017) 5579–5583.
- [27] R. Snoeckx, A. Bogaerts, Plasma technology - a novel solution for CO₂ conversion? *Chem. Soc. Rev.* 46 (2017) 5805–5863.
- [28] T. Nozaki, A. Ağiral, S. Yuzawa, J.G.E. Han Gardeniers, K. Okazaki, A single step methane conversion into synthetic fuels using microplasma reactor, *Chem. Eng. J.* 166 (2011) 288–293.
- [29] A. Indarto, H. Lee, J.W. Choi, H.K. Song, Partial oxidation of methane with yttria-stabilized zirconia catalyst in a dielectric barrier discharge, *Energy Sources Part A: Recovery Util. Environ. Eff.* 30 (2008) 1628–1636.
- [30] P. Chawdhury, D. Ray, C. Subrahmanyam, Single step conversion of methane to methanol assisted by nonthermal plasma, *Fuel Process. Technol.* 179 (2018) 32–41.
- [31] P. Chawdhury, D. Ray, T. Vinodkumar, C. Subrahmanyam, Catalytic DBD plasma approach for methane partial oxidation to methanol under ambient conditions, *Catal. Today* 337 (2019) 117–125.
- [32] P. Chawdhury, Y. Wang, D. Ray, S. Mathieu, N. Wang, J. Harding, F. Bin, X. Tu, C. Subrahmanyam, A promising plasma-catalytic approach towards single-step methane conversion to oxygenates at room temperature, *Appl. Catal. B: Environ.* 284 (2021), 119735.
- [33] B. Loenders, Y. Engelmann, A. Bogaerts, Plasma-catalytic partial oxidation of methane on Pt(111): a microkinetic study of the role of different plasma species, *J. Phys. Chem. C* 125 (2021) 2966–2983.
- [34] H. Puliyalil, D. Lašič Jurković, V.D.B.C. Dasireddy, B. Likozar, A review of plasma-assisted catalytic conversion of gaseous carbon dioxide and methane into value-added platform chemicals and fuels, *RSC Adv.* 8 (2018) 27481–27508.
- [35] D.W. Larkin, L.L. Lobban, R.G. Mallinson, The direct partial oxidation of methane to organic oxygenates using a dielectric barrier discharge reactor as a catalytic reactor analog, *Catal. Today* 71 (2001) 199–210.
- [36] L.M. Zhou, B. Xue, U. Kogelschatz, B. Eliasson, Partial oxidation of methane to methanol with oxygen or air in a nonequilibrium discharge plasma, *Plasma Chem. Plasma Process.* 18 (1998) 375–393.
- [37] P.G. Lustemberg, R.M. Palomino, R.A. Gutiérrez, D.C. Grinter, M. Vorokhta, Z. Liu, P.J. Ramírez, V. Matolín, M.V. Ganduglia-Pirovano, S.D. Senanayake, J. A. Rodríguez, Direct conversion of methane to methanol on Ni-Ceria surfaces: metal-support interactions and water-enabled catalytic conversion by site blocking, *J. Am. Chem. Soc.* 140 (2018) 7681–7687.
- [38] A.J. Knorpp, A.B. Pinar, M.A. Newton, V.L. Sushkevich, J.A. van Bokhoven, Copper-exchanged omega (MAZ) zeolite: copper-concentration dependent active sites and its unprecedented methane to methanol conversion, *ChemCatChem* 10 (2018) 5593–5596.
- [39] S. Pancheshnyi, B. Eismann, G.J.M. Hagelaar, L.C. Pitchford, Computer Code ZDPlasKin, University of Toulouse, LAPLACE, CNRS-UPS-INP, Toulouse, France, 2008. <http://www.zdplaskin.laplace.univ-tlse.fr>.
- [40] X. Zhu, P. Huo, Y.-p. Zhang, D. Cheng, C. Liu, Structure and reactivity of plasma treated Ni/Al₂O₃ catalyst for CO₂ reforming of methane, *Appl. Catal. B: Environ.* 81 (2008) 132–140.
- [41] D. Hu, J. Gao, Y. Ping, L. Jia, P. Gunawan, Z. Zhong, G. Xu, F. Gu, F. Su, Enhanced investigation of CO methanation over Ni/Al₂O₃ catalysts for synthetic natural gas production, *Ind. Eng. Chem. Res.* 51 (2012) 4875–4886.
- [42] A. Alihosseinzadeh, B. Nematollahi, M. Rezaei, E.N. Lay, CO methanation over Ni catalysts supported on high surface area mesoporous nanocrystalline γ-Al₂O₃ for CO removal in H₂-rich stream, *Int. J. Hydrog. Energy* 40 (2015) 1809–1819.
- [43] <https://xpsimplified.com/elements/nickel.php>.
- [44] S. Kikumakki, B. Shepizer, G. Sagar, K. Chary, A. Clearfield, Hydrogenation of naphthalene over NiO/SiO₂-Al₂O₃ catalysts: structure-activity correlation, *J. Catal.* 242 (2006) 319–331.
- [45] C.P. Li, A. Proctor, D.M. Hercules, Curve fitting analysis of ESCA Ni 2p spectra of nickel-oxygen compounds and Ni/Al₂O₃ catalysts, *Appl. Spectrosc. Rev.* 38 (1984) 880–886.
- [46] P. Salagre, J.L.G. Fierro, F. Medina, J.E. Sueiras, Characterization of nickel species on several γ-alumina supported nickel samples, *J. Mol. Catal. A: Chem.* 106 (1996) 125–134.
- [47] J. Jongsomjit, B. Jongsomjit, Catalytic ethanol dehydration to ethylene over nanocrystalline γ- and γ-Al₂O₃ catalysts, *J. Oleo Sci.* 66 (2017) 1029–1039.
- [48] Y. Jian, T. Yu, Z. Jiang, Y. Yu, M. Douthwaite, J. Liu, R. Albilali, C. He, In-depth understanding of the morphology effect of α-Fe₂O₃ on catalytic ethane destruction, *ACS Appl. Mater. Interfaces* 11 (2019) 11369–11383.
- [49] D.A. Erwin, J.A. Kunc, Electron-impact dissociation of the methane molecule into neutral fragments, *Phys. Rev. A* 72 (2005), 052719.
- [50] D.A. Erwin, J.A. Kunc, Dissociation and ionization of the methane molecule by nonrelativistic electrons including the near threshold region, *J. Appl. Phys.* 103 (2008), 064906.
- [51] C. De Bie, B. Verheyde, T. Martens, J. van Dijk, S. Paulussen, A. Bogaerts, Fluid modeling of the conversion of methane into higher hydrocarbons in an atmospheric pressure dielectric barrier discharge, *Plasma Process. Polym.* 8 (2011) 1033–1058.
- [52] C. De Bie, J. van Dijk, A. Bogaerts, The dominant pathways for the conversion of methane into oxygenates and syngas in an atmospheric pressure dielectric barrier discharge, *J. Phys. Chem. C* 119 (2015) 22331–22350.
- [53] R.E. Walkup, K.L. Saenger, G.S. Selwyn, Studies of atomic oxygen in O₂ + CF₄ rf discharges by two-photon laser-induced fluorescence and optical emission spectroscopy, *J. Chem. Phys.* 84 (1986) 2668–2674.
- [54] B. Eliasson, U. Kogelschatz, Electron impact dissociation in oxygen, *J. Phys. B: At. Mol. Opt. Phys.* 19 (1986) 1241–1247.
- [55] P.C. Cosby, Electron-impact dissociation of oxygen, *J. Chem. Phys.* 98 (1993) 9560–9569.
- [56] Q. Tang, Z. Shen, L. Huang, T. He, H. Adidharma, A.G. Russell, M. Fan, Synthesis of methanol from CO₂ hydrogenation promoted by dissociative adsorption of hydrogen on a Ga₃Ni₅(221) surface, *Phys. Chem. Chem. Phys.* 19 (2017) 18539–18555.
- [57] M. Shirazi, E.C. Neyts, A. Bogaerts, DFT study of Ni-catalyzed plasma dry reforming of methane, *Appl. Catal. B: Environ.* 205 (2017) 605–614.
- [58] S. Li, R. Ahmed, Y. Yi, A. Bogaerts, Methane to methanol through heterogeneous catalysis and plasma catalysis, *Catalysts* 11 (2021) 590.
- [59] V.L. Sushkevich, D. Palagin, M. Ranocchiari, J.A. van Bokhoven, Selective anaerobic oxidation of methane enables direct synthesis of methanol, *Science* 356 (2017) 523–527.
- [60] K. Narsimhan, K. Iyoki, K. Dinh, Y. Roman-Leshkov, Catalytic oxidation of methane into methanol over copper-exchanged zeolites with oxygen at low temperature, *ACS Cent. Sci.* 2 (2016) 424–429.